Review EL'BAHITH - ENS - Bouzareah - Algiers

ISSN : 9577-1112	EISSN : 2602-5388	Volume: (17)	Number : (02)	year: 2025	Pages: 117-134

Impact of Wildfires on Land cover in African Mediterranean forest: A case study of the august 2021 fire in Tizi Ouzou region (Algeria), using LANDSAT (8) satellite images

تأثير حرائق الغابات على الغطاء الأرضي في الغابات المتوسطية الأفريقية: دراسة حالة حريق أوت 2021 في منطقة تيزي وزو (الجزائر)، باستخدام صور القمر الاصطناعي لاند سات (08)

Mohamed Mezrag
Higher School of Teachers Training, Bouzareah, Algiers, Algeria
mezreg.mohamed@ensb.dz

Omar Temelghaghet
Higher School of Teachers Training, Bouzareah, Algiers, Algeria
temelghaghet.omar@ensb.dz

Date of receipt: 16/05/2025 Date of acceptance: 12/09/2025 Date of publication: 30/09/2025

First Corresponding author: Mohamed Mezra, mezreg.mohamed@ensb.dz
Second Corresponding author: Omar Temelghaghet temelghaghet.omar@ensb.dz

ملخص:

تبحث هذه الدراسة في تأثير حرائق الغابات التي اجتاحت منطقة تيزي وزو في الأطلس التلي الشرقي بالجزائر في 8 أغسطس 2021. وقد أتت الحرائق على ما يقرب من 506.3 كيلومتر مربع، مما دفع إلى إجراء تحليل يستند إلى صور القمر الصناعي لاندسات 8 باستخدام نسبة الحرق الطبيعية (NBR) ومؤشر الغطاء النباتي المتباين الطبيعي (NDVI) و نسبة الحرق الطبيعية المتباينة (dNBR). وقد قيم البحث شدة أضرار الحرائق عبر ستة أنواع سائدة من الغطاء الأرضي في منطقة الدراسة وتتبع مستويات تعافيها على مدى عامين بعد الحادث. وقد تم اختيار اثنين وأربعين نقطة عينة عشوائية من هذه الأنواع من الغطاء الأرضي، تمثل حوالي 95٪ من السمات الأساسية داخل المناطق المتضررة. وقد تم تحديد ارتباط إيجابي قوي ($R^2 = 0.918$) بين dNBR وdNDVI، مما يوفر نظرة جيدة لاتجاهات شدة الحرائق المصنفة من مناطق عالية ومتوسطة الخطورة إلى مناطق منخفضة الخطورة. أظهرت بيانات مؤشرَي الغطاء النباتي الطبيعي (NBR) والغطاء النباتي الطبيعي (NDVI) أن أشجار الفاكهة، وخاصةً بساتين الزيتون، تكبدت أكبر خسارة بعد الحريق، حيث انخفضت قيم الانعكاس بنسبة -120.80% لمؤشر الغطاء النباتي الطبيعي (NBR) و-78.30% لمؤشر الغطاء النباتي الطبيعي (NDVI). في المقابل، بعد عامين من الحريق، أظهرت مؤشرات الغطاء النباتي الطبيعي (NDVI) تعافيًا تدريجيًا في جميع أنواع الغطاء الأرضي، مسجلةً متوسط استعادة بنسبة 16.31% مقارنةً بقيم مؤشر الغطاء النباتي الطبيعي الحرجة بعد الحريق والبالغة -75.92%.

الكلمات المفتاحية:

لاندسات8؛ مؤشر نسب الحرق الطبيعية (NBR)؛ مؤشر الغطاء النباتي (NDVI)؛ شدة الحرق؛ مؤشر الحرق الطبيعي المتباين (dNBR).

Review EL'BAHITH - ENS - Bouzareah - Algiers					
ISSN : 9577-1112	EISSN : 2602-5388	Volume: (17)	Number : (02)	year: 2025	Pages: 117-134

Abstract:

This study investigates the impact of the wildfire that swept through the Tizi Ouzou region in Algeria's eastern Tell Atlas on August 8, 2021. The fire ravaged approximately 506.3 km², prompting an analysis based on Landsat 8 satellite imagery using the Normalized Burn Ratio (NBR), Normalized Differenced Vegetation Index (NDVI), and Differenced Normalized Burn Ratio (dNBR). The research assessed the severity of fire damage across six predominant land cover types in the study area and tracked their recovery levels over a two-year span following the incident. Forty-two random sample points were selected from these land cover types, representing about 95% of the primary features within the affected areas. A strong positive correlation ($R^2 = 0.918$) was identified between dNBR and dNDVI, offering insight into burn severity trends categorized from high and moderate risk to low-risk zones. Data from NBR and NDVI indices revealed that fruit trees, particularly olive orchards, suffered the most significant post-fire loss, with reflectance values declining by -120.80% for NBR and -78.30% for NDVI. By contrast, two years after the fire, NDVI indices demonstrated gradual recovery across land cover types, marking an average restoration of 16.31% compared to the critical post-fire NDVI values of -75.92%.

Keywords:

Landsat8 ; Normalized Burn Ratio (NBR) ; Normalized Differenced Vegetation Index (NDVI); Burn Severity ; Differenced Normalized Burn Ratio.

1. ***INTRODUCTION*** :

In recent years, forests across various regions such as Australia, California, Chile, and Southern Europe, have experienced devastating wildfire disasters, resulting in severe environmental, economic, and human damages (Bowman et al., 2020; Keeley, Bond, Bradstock, Pausas, & Rundel, 2011). Similarly, Algeria's northern coastal areas, part of the Mediterranean forest ecosystem, have faced recurrent wildfires that significantly affect not only the overall ecosystem but also specific aspects like land cover. These fires frequently contribute to harmful outcomes such as biodiversity loss, accelerated desertification, and exacerbation of climate change. In central Algeria, forest coverage spans approximately 446,936 hectares, of which around 10% (44,300 hectares) were degraded by wildfires between 2008 and 2017 (Nouar, Saifi, & Ahmed, 2022). The northeastern coastal provinces—ranging from Tizi Ouzou to El Tarf, are particularly vulnerable to these recurring wildfire events (Mondiale, 2023), with most fires reportedly having unknown causes (Madoui, 2002).

Tizi Ouzou, located in the eastern Tell Atlas region of Algeria and covering an area of roughly 2,970 square kilometers, is characterized by a Mediterranean climate. This region features diverse land cover types with fruit trees like olive trees dominating the landscape at an estimated 69.86% (350 square kilometers), followed by mixed crops and pastures at 3.59% (18 square kilometers), crops at 5.58% (28 square kilometers), a combination of sparse and dense forests at 16.76% (84 square kilometers), and pastures at 4.19% (21 square kilometers). Tizi Ouzou experiences annual wildfires, particularly during the dry summer months when high temperatures and insufficient rainfall significantly increase vegetation dryness. One of the most devastating fires in this region occurred between August 8 and August 14, 2021. This fire destroyed approximately 506.3 square kilometers of land, heavily impacting the southern areas as well as parts of its central, northern, and northeastern territories.

In recent decades, advancements in remote sensing have enabled precise long-term monitoring of forest disturbances. Such techniques leverage high-resolution data sources like the Landsat image archive, established in 2008 (Yin, He, Fan, & Chen, 2024). Remote sensing methods provide the advantage of quickly identifying burnt areas over large geographic scales (Indratmoko & Rizqihandari, 2019). Research has highlighted various remote sensing products utilized to evaluate wildfire impacts, including Landsat imagery (Chen, Moriya, Sakai, Koyama, & Cao, 2016; Indratmoko & Rizqihandari, 2019), MODIS data (Giglio, Boschetti, Roy, Humber, & Justice, 2018), Sentinel-2 imagery (Roteta, Bastarrika, Padilla, Storm, & Chuvieco, 2019), Sentinel-1 data (Belenguer-Plomer, Tanase, Fernandez-Carrillo, & Chuvieco, 2019), and Synthetic Aperture Radar (SAR) imagery (Chini et al., 2019). Landsat data has proven particularly effective in mapping land cover and analyzing biophysical and geophysical characteristics of surface areas (Hansen & Loveland, 2012; Wulder, Masek, Cohen, Loveland, & Woodcock, 2012).

The Landsat 8 satellite images—which became available in 2013—are instrumental for tracking changes in land cover over time due to their multi-spectral capabilities. These images capture data across visible light spectra as well as near-infrared and thermal infrared bands. This makes them valuable for monitoring vegetation changes caused by fires and assessing recovery processes. Understanding patterns of land use and land cover change is vital for the effective management and sustainable development of natural resources (Myers, 1993). In this regard, connecting land cover dynamics with community livelihoods—whether urban or rural—is especially critical for planning and managing land use through remote sensing technologies.

This study aims to utilize multi-temporal Landsat 8 data to monitor land cover dynamics and assess health conditions before and after wildfire events. It seeks to determine whether spatial patterns have shifted or remained consistent due to fire impacts. Analysis methods employed include the Normalized Burn Ratio (NBR) and Normalized Difference Vegetation Index (NDVI) for burn severity assessment. Furthermore, Differential Normalized Burn Ratio (dNBR) was used to evaluate burn severity and quantify the damage across six distinct land cover types found within the study area. The dNBR serves as a key metric for understanding wildfire impacts (Parks, Dillon, & Miller, 2014; Rozario, Madurapperuma, & Wang, 2018).

2. *Study Area* :

The study area is located in northern Algeria, between the latitudes 36°27'00" N and 36°54'41" N, and longitudes 3°42'59" E and 5°39'19" E. It covers an area of 2,970 km² and includes 68 municipalities (Figure 1). The topography of the area is characterized by mountains with rugged terrain, as well as plateaus and plains that form extensive flat areas. The region is also traversed by several valleys. The climate of the Tizi Ouzou region is Mediterranean, with hot and dry summers, where the average maximum temperatures generally range between 30°C and 35°C, and can sometimes exceed 40°C during heatwaves. While winters are usually mild and wet. The study area is marked by various vegetation covers including forests with different species such as pine, oak, cypress, and cedar. Most of these forests are classified as biosphere reserves (Nouar, Saifi, & Ahmed, 2022). The region also includes vast areas of pastures and agricultural land, where various crops such as olive trees, cereals, fruits, and vegetables are cultivated. In addition, wild grasses and plants contribute to the biodiversity of the area.

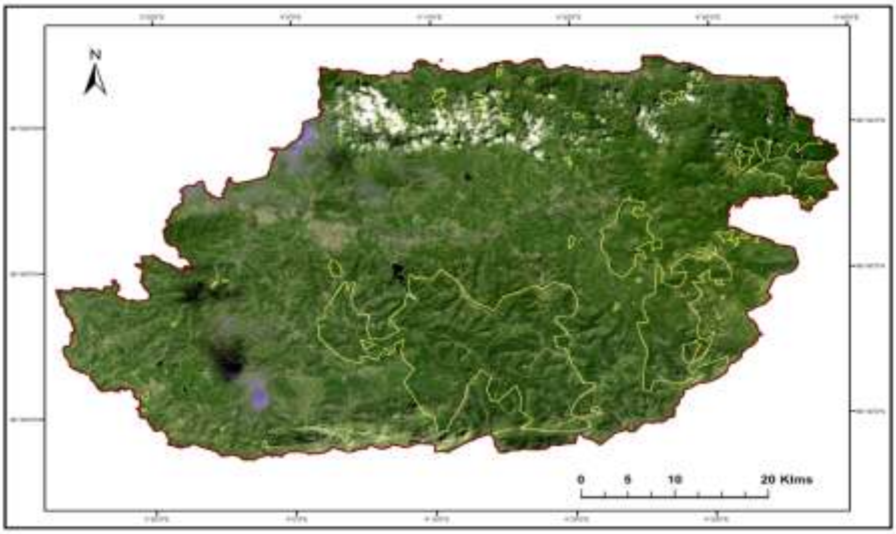

Fig.1. Map of the location of the study area (Tizi Ouazou)

3. *Data and methodology*:

3.1. Fire Perimeter : The fire perimeter of the Tizi Ouzou region was extracted by creating a color composite using bands 3, 4, and 5, based on two images of Landsat 8 satellite data captured on August 30, 2021. The images were first subjected to geometric and radiometric corrections. The burned areas, which appear in dark gray, were then digitized using ArcGIS software and saved in a digital file for subsequent processing.

Figure 02 shows that the fire significantly affected the southern part of the region, starting from its center, as well as parts of the northern and northeastern areas. The red color in the image highlight vegetation that was not affected by the fire.

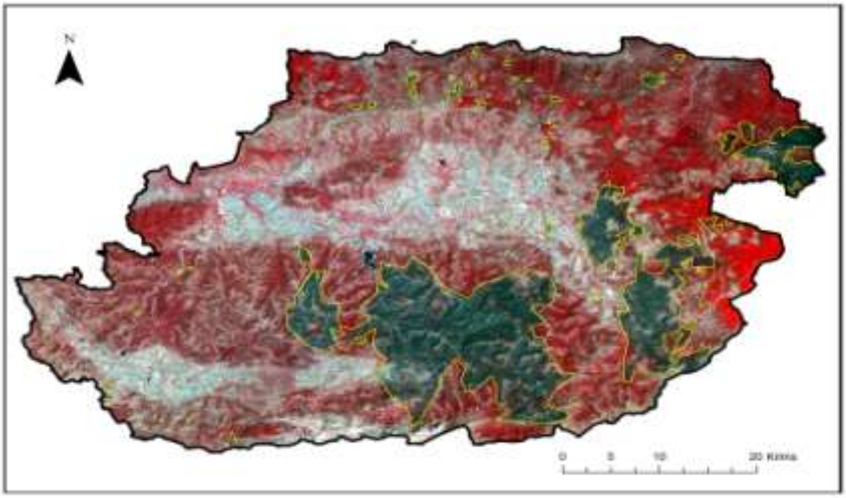

Fig.2. Limits of the burned area Province)

3.2. The Data :

a. Satellite Images : The images used to monitor and assess the effects of the fire (August 8, 2021) were downloaded from the USGS website(https://earthexplorer.usgs.gov), specifically from the Landsat 8 Operational Land Imager (OLI) and Thermal Infrared Sensor (TIRS). The characteristics of the used images are presented in Table 01.

Band Number	Description	Wavelength	Resolution
Band 1	Coastal / Aerosol	0.433 to 0.453 µm	30 meter
Band 2	Visible blue	0.450 to 0.515 µm	30 meter
Band 3	Visible green	0.525 to 0.600 µm	30 meter
Band 4	Visible red	0.630 to 0.680 µm	30 meter
Band 5	Near-infrared	0.845 to 0.885 µm	30 meter
Band 6	Short wavelength infrared	1.56 to 1.66 µm	30 meter
Band 7	Short wavelength infrared	2.10 to 2.30 µm	60 meter
Band 8	Panchromatic	0.50 to 0.68 µm	15 meter
Band 9	Cirrus	1.36 to 1.39 µm	30 meter
Band 10	Long wavelength infrared	10.3 to 11.3 µm	100 meter
Band 11	Long wavelength infrared	11.5 to 12.5 µm	100 meter

Table 1 : *Landsat-8 OLI & TIRS Sensors*

Souce : https://gisgeography.com/landsat-8-bands-combinations/

Table 02 shows the description of the images used in this study. A selection of images before and after the fire was chosen with the following dates: April 8, 2021; August 30, 2021; April 11, 2022; and April 6, 2023. Images were selected in April to ensure a good reading of vegetation index values and to minimize cloud cover in the study area.

All raw images were processed using ArcGIS software. The bands were combined to create natural color composite images using bands 2, 3, and 4 (Red, Green, Blue). Additionally, for post-fire comparison, composite images were created using bands 7, 5, and 1 (SWIR). The significance of SWIR images lies in their ability to highlight features that cannot be detected using natural color composites or false-color infrared images.

After extracting the natural color images, the digital file of the fire perimeter was used to clip each processed image, isolating the areas affected by the fire for comparison and assessment.

Official name of data set	*Projection system*	*Acquisition Dates*	*Post-Fire Days*
LC08_L2SP_195035_20210408_20210416_02_T1	WGS 1984 UTM Zone 31N	9 April 2021	-122
LC08_L2SP_195035_20210830_20210909_02_T1	WGS 1984 UTM Zone 31N	29 August 2021	+22
LC08_L2SP_195035_20220411_20220419_02_T1	WGS 1984 UTM Zone 31N	12 April 2022	+245
LC09_L2SP_195035_20230406_20230408_02_T1	WGS 1984 UTM Zone 31N	7 April 2023	605

Table 2 : The time-series Landsat 8 image data used in this study

b. *Land Cover Database* :

The land cover database for the Tizi Ouzou region was obtained based on the land use map created by the Engineering and Studies Officer (Algeria), prior to the fire event. This data was processed using ArcGIS software to generate a digital map (Figure 3) containing a new layer composed of six land cover types. These types were used to compare the evolution of land cover within the fire-affected area before and after the fire.

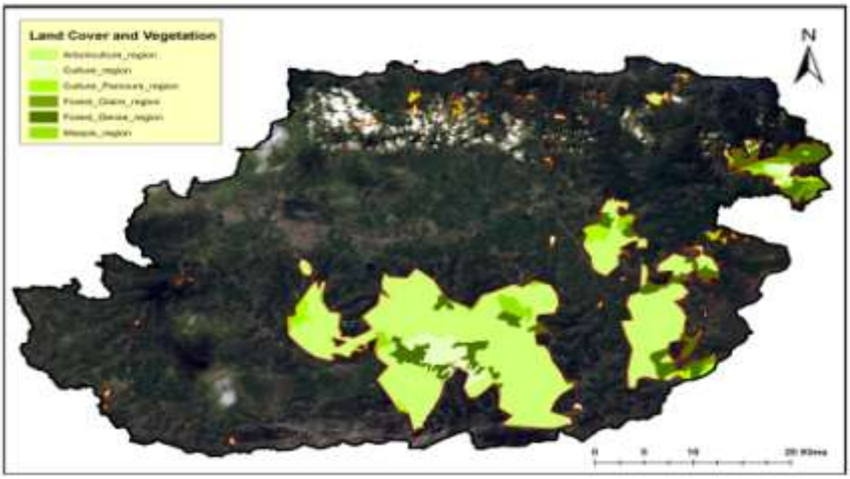

Fig.3. NCLD 2016

ISSN : 9577-1112	EISSN : 2602-5388	Volume: (17)	Number : (02)	year: 2025	Pages: 117-134

3.3. *Methodology* :

The first step involves downloading the Landsat 8 satellite images, followed by stacking the necessary bands to extract images for the NDVI and the NBR. The processing steps for extracting these indices are simplified in Figure 04.

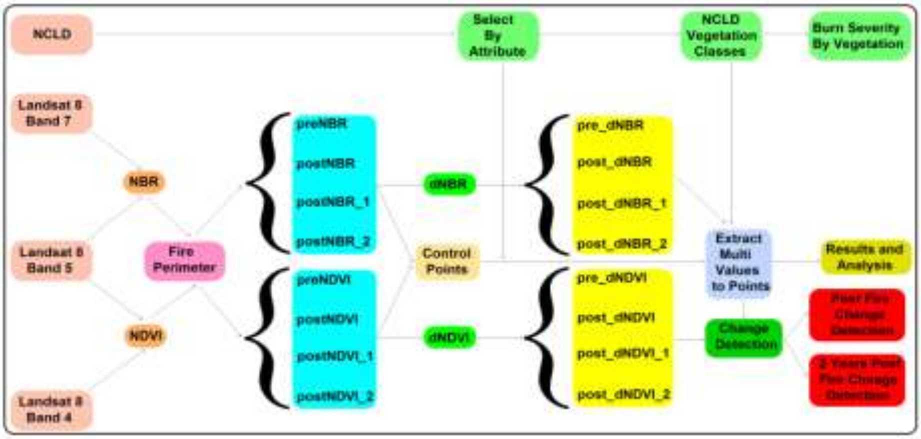

Fig.4. Geoprocessing Model used for this study

- Normalized Difference Vegetation Index (NDVI) : The NDVI values range between -1 and 1. Values from 0 to 1 correspond to water, snow, or clouds, while barren land values are close to 0. Sparse vegetation or grasslands range from 0.1 to 0.5, and grass and shrub lands have values between 0.4 and 0.5. Dense vegetation and forests have values higher than 0.5. To calculate the NDVI for the selected dates, the near-infrared band (IR5) and the red band (Band 4) were used, according to the following formula :

$$NDVI = \frac{(Band\ 5 - Band\ 4)}{(Band\ 5 + Band\ 4)}$$

- Natural Burn Ratio (NBR) : To extract the natural burn ratio for the images, the near-infrared band (IR 5) and the short-wave infrared band (SWIR 7) were used, based on the following formula :

$$NBR = \frac{(IR - SWIR)}{(IR + SWIR)}$$

- *Differenced Burn Ratio and NDVI (dNBR and dNDVI)*:

The differenced indices were derived from the outputs of the natural burn ratio and the vegetation index difference. To determine the intensity of the burn in the study area, the differenced natural burn ratio (dNBR) was used. The United States Geological Survey (USGS) developed a scale to show the varying degrees of burn severity (Table 3). These levels are extremely useful for post-fire land management and allow authorities to evaluate the potential for vegetation and ecosystem recovery.

The differenced burn ratio for the years 30/08/2021, 11/04/2022, and 06/04/2023 were calculated by subtracting each post-fire image from the corresponding pre-fire image. The first image, taken 22 days after the fire, and the two others, from April of the first and second years after the fire, were processed in the same way to obtain the differenced indices.

Digital processing with ArcGIS allowed us to obtain three images of the differenced natural burn ratio indices and three images of the differenced vegetation index indices after the fire. These images will assist in tracking the restoration of land cover over time.

Severity Level	*Severity Level dNBR Range*	*dNBR Range (Not Scaled)*
	Enhanced Regrowth, High	Inf. to -0.251
	Enhanced Regrowth, Low	-.250 – -0.101
	Unburned	-0.100 – 0.99
	Low Severity	0.100 – 0.269
	Moderate Low Severity	0.270 – 0.439
	Moderate High Severity	0.440 – 0.659
	High Severity	Sup. to 0.660

Table 3 : Burn Severity Levels

- *Sampling Points* :

To extract the values of NDVI, NBR, dNDVI, and dNBR, we selected a set of sampling points distributed across the six land cover types in the study area. A total of 42 sampling points were established, with seven points per land cover type. This will help achieve the first goal of identifying the areas with the highest vegetation loss and recovery post-fire (Figure 05).

The values of the sampling points were saved in Excel tables (Appendix A) for further analysis. These values were used to generate scatterplot charts and point line charts to analyze and interpret the results.

Review EL'BAHITH - ENS - Bouzareah - Algiers

ISSN : 9577-1112	EISSN : 2602-5388	Volume: (17)	Number : (02)	year: 2025	Pages: 117-134

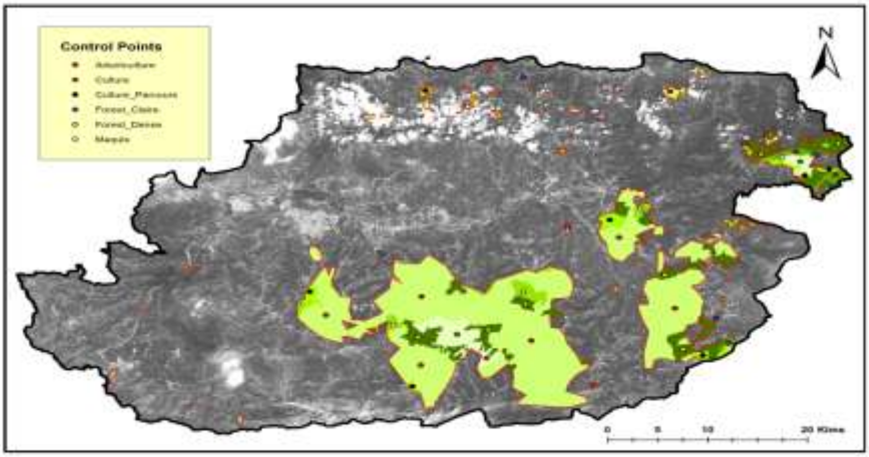

Fig.5. Control Point Locations in the Study Area

- **Tracking Changes**: The second goal of the study was to examine how the study area changed before and after the fire, and to identify which land cover type recovered most quickly. NDVI images, with reflectance values ranging from -1 to 1, were categorized into six groups. According to a study by Akbar et al. (2019), the acceptable values for land cover types were classified as follows: water (-0.28 to -0.015), built-up areas (0.015 to 0.14), barren land (0.14 to 0.18), shrub land (0.18 to 0.27), sparse vegetation (0.27 to 0.36), and dense vegetation (0.36 to 0.74).

Each NDVI image was classified and reclassified into tables linked to the pixel values for each classified range. This simple reclassification produced a raster with an attribute table showing the total pixel count for each classified value. Additionally, a new column was added to track the recovered and lost areas for each land cover type.

4. ***Results and Discussion*** :

4.1. Natural Burn Ratio (NBR) : A previous study by S. Escuin (2008) compared and explained the use of NBR in determining fire severity levels for three separate fires that occurred in southern Spain. This study showed a good correlation between the pre- and post-fire NBR values, effectively identifying fire severity levels. Visual inspection of Figures 6 and 7 illustrates the state of the study area two years after the fire, showing the gradual recovery of land cover. The average NBR values increased from 0.0638 in the first year to 0.1525 in the second year, indicating a notable improvement in land cover within the study area.

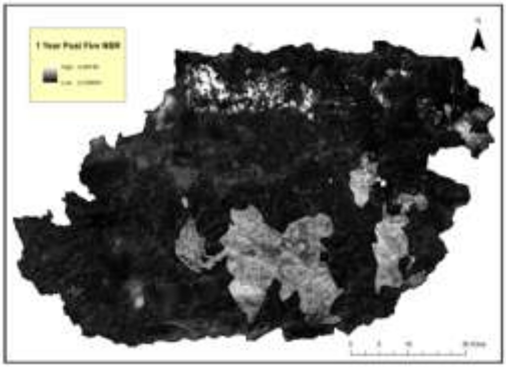

Fig.6. NBR for year one post fire

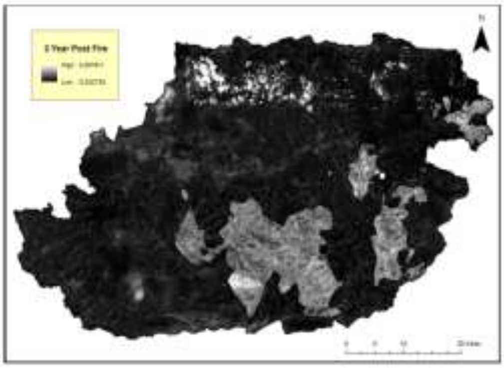

Fig.7. NBR for year two post fire

4.2. Burn Severity : To determine burn severity, the pre-fire NBR was subtracted from the post-fire NBR, resulting in the differenced NBR (dNBR). For this, the image taken on April 9, 2021, was subtracted from the image taken on August 29, 2021, approximately 22 days post-fire (Figure 8). Burn severity levels in the study area were classified using the UN-SPIDER classification, developed by the United Nations Office for Outer Space Affairs. The results in Table 4 show that the burned area was approximately 505 km², with 150 km² classified as highly to moderately burned, 174 km² moderately to low burned, 114 km² low burned, and 67 km² as unburned. The unburned areas showed rapid natural recovery.

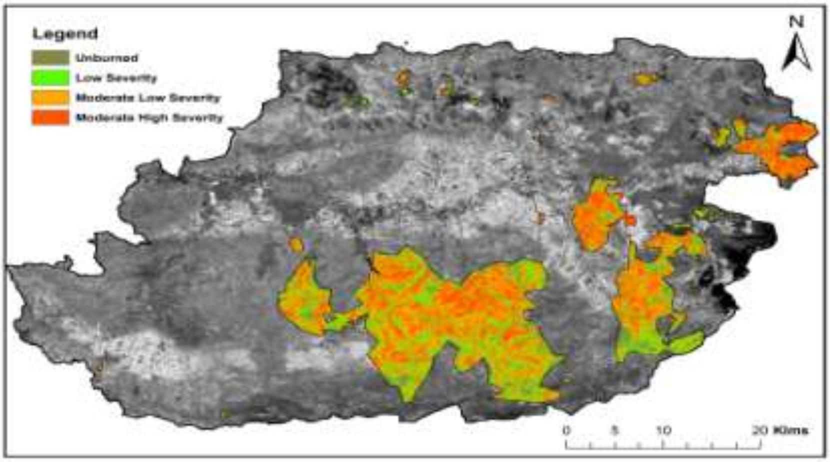

Fig.8. Burn Severity Index

The table 4 also provides results on the burn severity experienced by each type of land cover within the study area approximately 22 days after the fire. Olive trees were the most affected, covering about 350 km², followed by dense and sparse forests combined, covering a total of 94 km². The remaining land cover types were affected over smaller, similar-sized areas. Additionally, figure 8 illustrates the extent of the burned land.

Vegetation	Burn Severity in Km2			
	Unburned	Low Severity	Moderate Low Severity	Moderate High Severity
Arboriculture	46	80	124	100
Culture_Parcours	3	4	5	6
Culture	3	6	10	9
Forest_Claire	1	1	2	6
Forest_Dense	11	17	24	22
Maquis	3	5	7	6

Table 4 : Burn Severity by Vegetation Class (Acres)

4.3. Vegetation Index : After the digital processing of Landsat satellite images using ArcGIS software and their reclassification, vegetation index results were obtained (Table 5). The analysis shows that the NDVI values for the pre-fire image (April 8, 2021) ranged from 0.5733 to -0.042, with an average of 0.2656. The post-fire image, taken 22 days later, showed values between 0.4422 and -0.1046, with an average of 0.1688, indicating unhealthy vegetation conditions. One-year post-fire, the NDVI values increased slightly to an average of 0.277, showing a recovery of vegetation cover. In the second year after the fire, the NDVI average slightly decreased to 0.2351, reflecting a decline due to increased temperatures and drought, which negatively impacted vegetation recovery.

Acquisition Dates	High values	Low values	Average values
9 April 2021	0.5733	-0.042	0.26565
29 August 2021	0.4422	-0.1046	0.1688
12 April 2022	0.5409	0.0131	0.277
7 April 2023	0.5668	-0.0965	0.23515

Table 5 : Reclassified NDVI

4.4. Statistical Results of Burn and Vegetation Indices :

The statistical results of the control point value (NDVI, NBR, and their differenced versions) over the years (Appendix A) show the following :

- There is a strong correlation between NBR and NDVI values. The correlation coefficient (R^2) before the fire was 0.918. After each year, the correlation between these indices increased, indicating the gradual recovery of vegetation in the study area (Table 6).

Acquisition Dates	9 April 2021	29 August 2021	12 April 2022	7 April 2023
correlation R^2	**0.918**	**0.936**	**0.991**	**0.937**

Tab 6 : Yearly NBR/NDVI R^2 Correlation

- For olive trees, the pre-fire NDVI value was 0.34 for the average of seven control points, while it dropped to 0.07 immediately after the fire, representing a decline of 78.3%. This indicates that this plant type was heavily affected by the fire. Other land cover types also experienced varying degrees of decline, with dense and sparse forests decreasing by 78.5% and 80%, respectively, and agricultural areas, grasslands, and shrublands decreasing by 72.1%, 71.5%, and 75.2%.

- Two years after the fire, the land cover types began showing gradual recovery. The olive trees increased by 10.5% to a value of 0.33. The dense and sparse forests increased by 15.9% and 41.6%, respectively. Agricultural areas, grasslands, and shrublands increased by 4.4%, 4.1%, and 21.4%, respectively.

5. Conclusion:

This study aims to monitor the substantial changes in land cover within the designated study area, with an emphasis on the recovery of land cover and the degree of transformation observed over a two-year period. By analyzing a series of Landsat satellite images captured before and after a fire event, the research provides insights into these dynamics. To achieve its objectives, the study utilized the Normalized Burn Ratio (NBR) and the Normalized Difference Vegetation Index (NDVI), generating a series of geospatial images and employing pre-fire land use maps to identify monitoring points. Digital layers for distinct land cover types were created, facilitating a comprehensive analysis. The findings indicated a strong correlation between the two indices across all images, reflected by a coefficient exceeding $R^2 = 0.90$. The examination of control points across six land cover types revealed significant damage immediately after the fire, as evidenced by NDVI values dropping between 71.0% and 80.0%. Nonetheless, two years post-fire, all land cover types showed signs of recovery, with NDVI improvements varying from 4.0% to 42.0%. Further analysis using the NBR index was conducted pre- and post-fire to evaluate burn severity across the region. Results demonstrated that most areas experienced burn impacts ranging from moderate to high severity, as well as low to moderate severity, based on Differenced NBR (dNBR) classifications established by the United States Geological Survey (USGS). Integrating dNBR outcomes with land use maps allowed for precise determination of burn severity across different land cover types. In conclusion, leveraging Landsat 8 imagery to assess fire impacts on land cover provides meaningful insights into the environmental consequences of forest fires in fire-prone areas, particularly in eastern Algeria's Tizi Ouzou region. The findings underscore the critical importance of land management practices, restoration efforts, protective measures, and fire risk prevention strategies to mitigate long-term environmental impacts.

6. References:

Akbar, Tahir & Hassan, Quazi & Ishaq, Sana & Batool, Maleeha & Butt, Hira & Jabbar, Hira. (2019). Investigative Spatial Distribution and Modelling of Existing and Future Urban Land Changes and Its Impact on Urbanization and Economy. Remote Sensing. 11. 105. 10.3390/rs11020105.

Belenguer-Plomer, M. A., Tanase, M. A., Fernandez-Carrillo, A., & Chuvieco, E. (2019). Burned area detection and mapping using Sentinel-1 backscatter coefficient and thermal anomalies. Remote sensing of environment, 233, 111345 .

Bowman, D. M., Kolden, C .A., Abatzoglou, J. T., Johnston, F. H., van der Werf, G. R., & Flannigan, M. (2020). Vegetation fires in the Anthropocene. Nature Reviews Earth & Environment, 1(10), 500-515 .

Cahyono, B. E., Fibyana, V., Nugroho, A. T., & Subekti, A. (2021). Mapping and analysis burned area based on LANDSAT 8 OLI/TIRS and hotspots data in palangkaraya of central kalimantan province-Indonesia. Paper presented at the Journal of Physics: Conference Series.

Chen, W., Moriya, K., Sakai, T., Koyama, L., & Cao, C. (2016). Mapping a burned forest area from Landsat TM data by multiple methods. Geomatics, Natural Hazards and Risk, 7(1), 384-402 .

Chini, M., Pelich, R., Pulvirenti, L., Pierdicca, N., Hostache, R., & Matgen, P. (2019). Sentinel-1 InSAR coherence to detect floodwater in urban areas: Houston and Hurricane Harvey as a test case. Remote Sensing, 11(2), 107 .

Escuin, S., R. Navarro & P. Fernández (2008) Fire severity assessment by using NBR(Normalized Burn Ratio) and NDVI (Normalized Difference Vegetation Index) derived from LANDSAT TM/ETM images, International Journal of Remote Sensing, 29:4, 1053- 1073, DOI: 10.1080/01431160701281072

Giglio, L., Boschetti, L., Roy, D. P., Humber, M. L., & Justice, C. O. (2018). The Collection 6 MODIS burned area mapping algorithm and product. Remote sensing of environment, 217, 72-85 .

Hansen, M. C., & Loveland, T. R. (2012). A review of large area monitoring of land cover change using Landsat data. Remote sensing of environment, 122, 66-74 .

Indratmoko, S., & Rizqihandari, N. (2019). Burn area detection using Landsat 8 OLI TIRS. Paper presented at the IOP Conference Series: Earth and Environmental Science.

Keeley, J. E., Bond, W. J., Bradstock, R. A., Pausas, J. G., & Rundel, P. W. (2011). Fire in Mediterranean ecosystems: ecology, evolution and management .

Madoui, A. (2002). Les incendies de forêt en Algérie. Historique, bilan et analyse. Forêt méditerranéenne, 23(1), 23-30 .

mondiale, l. B. (2023). NOTE SUR LES FORÊTS ALGÉRIENNES Gestion durable des forêts pour lutter contre les feux de forêts© 2023 Banque internationale pour la reconstruction et le développement/Banque mondiale. Retrieved from

Myers, N. (1993). Tropical forests: the main deforestation fronts. Environmental conservation, 20(1), 9-16 .

Nouar, B., Saifi, M., & Ahmed, B. (2022). Evaluation et cartographie des feux de forêts généralisés d’août 2021 à Bejaia et Tizi Ouzou: Approche géomatique. Journal Algérien des Régions Arides, 14(2), 60-67 .

Parks, S. A., Dillon, G. K., & Miller, C. (2014). A new metric for quantifying burn severity: the relativized burn ratio. Remote Sensing, 6(3), 1827-1844 .

Roteta, E., Bastarrika, A., Padilla, M., Storm, T., & Chuvieco, E. (2019). Development of a Sentinel-2 burned area algorithm: Generation of a small fire database for sub-Saharan Africa. Remote sensing of environment, 222, 1-17 .

Rozario, P. F., Madurapperuma, B. D., & Wang, Y. (2018). Remote sensing approach to detect burn severity risk zones in Palo Verde National Park, Costa Rica. Remote Sensing, 10(9), 1427 .

Wulder, M. A., Masek, J. G., Cohen, W. B., Loveland, T. R., & Woodcock, C. E. (2012). Opening the archive: How free data has enabled the science and monitoring promise of Landsat. Remote sensing of environment .10-2 ،122 ،

Yin, J., He, B., Fan, C., & Chen, R. (2024). Fire has become a major disturbance agent in the forests of Southwest China. Ecological Indicators, 160, 111885 .

United Nations. Office for Outer Space Affairs UN-SPIDER knowledge Portal.< https://un-spider.org/advisory-support/recommended-practices/recommended-practiceburn-severity/in-detail/normalized-burn-ratio >

USGS. Landsat Normalized Burn Ratio. <https://www.usgs.gov/landsat-missions/landsat-normalized-burn-ratio >.

ISSN : 9577-1112 | EISSN : 2602-5388 | Volume: (17) | Number : (02) | year: 2025 | Pages: 117-134

Appendix A :

Arboriculture Control Points Table								
	April 8, 2021		October 30, 2021		April 11, 2022		April 6, 2023	
Control Points	Pre NBR	Pre NDVI	Post NBR	Post NDVI	NBRp 1	NDVIp 1	NBRp 2	NDVIp 2
1	0.20	0.28	-0.09	0.11	0.09	0.12	0.30	0.33
2	0.07	0.18	-0.11	0.10	-0.11	0.14	0.06	0.15
3	0.33	0.38	-0.12	0.04	-0.11	0.29	0.25	0.34
4	0.38	0.43	-0.10	0.06	-0.09	0.35	0.43	0.45
5	0.26	0.33	-0.13	0.09	-0.09	0.10	0.22	0.30
6	0.33	0.37	-0.14	0.11	0.09	0.25	0.25	0.29
7	0.36	0.40	-0.12	0.05	-0.12	0.08	0.25	0.27
	0.28	0.34	-0.12	0.08	-0.05	0.19	0.25	0.30
Year over Year Increase			-141.71%	-76.41%	-57.81%	137.49%	-618.90%	59.70%

Culture Control Points Table								
	April 8, 2021		October 30, 2021		April 11, 2022		April 6, 2023	
Control Points	Pre NBR	Pre NDVI	Post NBR	Post NDVI	NBRp 1	NDVIp 1	NBRp 2	NDVIp 2
1	0.35	0.40	-0.08	0.12	0.21	0.29	0.33	0.33
2	0.29	0.35	-0.08	0.14	0.13	0.27	0.20	0.32
3	0.26	0.34	-0.06	0.12	0.10	0.24	0.21	0.30
4	0.32	0.37	-0.06	0.24	0.17	0.29	0.31	0.34
5	0.34	0.40	-0.11	0.11	0.15	0.24	0.23	0.31
6	0.35	0.40	-0.01	0.10	0.11	0.28	0.25	0.33
7	0.28	0.33	-0.10	0.09	0.09	0.15	0.25	0.25
	0.31	0.37	-0.07	0.13	0.14	0.25	0.25	0.31
Year over Year Increase			-123.12%	-64.21%	-290.68%	90.18%	84.29%	24.20%

Culture_Background Control Points Table								
	April 8, 2021		October 30, 2021		April 11, 2022		April 6, 2023	
Control Points	Pre NBR	Pre NDVI	Post NBR	Post NDVI	NBRp 1	NDVIp 1	NBRp 2	NDVIp 2
1	0.35	0.41	-0.09	0.11	0.39	0.37	0.39	0.42
2	0.22	0.28	0.04	0.11	0.22	0.23	0.18	0.29
3	0.14	0.24	0.02	0.11	0.11	0.19	0.10	0.22
4	0.12	0.22	-0.07	0.10	0.08	0.17	0.08	0.19
5	0.30	0.37	-0.09	0.12	0.23	0.25	0.24	0.31
6	0.31	0.36	0.03	0.10	0.25	0.20	0.22	0.22
7	0.28	0.34	-0.16	0.10	0.04	0.17	0.18	0.26
	0.24	0.32	-0.04	0.11	0.19	0.23	0.20	0.27
Year over Year Increase			-117.79%	-65.70%	-532.68%	108.69%	5.55%	20.41%

Clear Forest Control Points Table								
	April 8, 2021		October 30, 2021		April 11, 2022		April 6, 2023	
Control Points	Pre NBR	Pre NDVI	Post NBR	Post NDVI	NBRp 1	NDVIp 1	NBRp 2	NDVIp 2
1	0.21	0.27	-0.08	0.09	0.12	0.17	0.20	0.25
2	0.30	0.36	-0.16	0.09	0.02	0.19	0.20	0.29
3	0.31	0.35	-0.16	0.11	0.08	0.20	0.20	0.30
4	0.18	0.26	-0.14	0.11	0.06	0.17	0.12	0.23
5	0.28	0.34	-0.16	0.10	0.06	0.18	0.18	0.27
6	0.10	0.20	-0.03	0.10	0.09	0.17	0.07	0.18
7	0.26	0.33	-0.13	0.11	0.17	0.28	0.24	0.29
	0.23	0.30	-0.12	0.10	0.09	0.19	0.17	0.26
Year over Year Increase			-152.74%	-66.47%	-170.50%	92.09%	99.85%	32.37%

Dense Forest Control Points Table								
	April 8, 2021		October 30, 2021		April 11, 2022		April 6, 2023	
Control Points	Pre NBR	Pre NDVI	Post NBR	Post NDVI	NBRp 1	NDVIp 1	NBRp 2	NDVIp 2
1	0.31	0.38	-0.05	0.13	0.32	0.25	0.20	0.29
2	0.26	0.30	-0.07	0.10	0.13	0.28	0.18	0.30
3	0.26	0.31	-0.15	0.11	0.07	0.19	0.21	0.25
4	0.23	0.28	-0.12	0.09	0.05	0.17	0.24	0.30
5	0.25	0.32	-0.14	0.10	0.32	0.27	0.21	0.30
6	0.26	0.31	-0.18	0.15	0.03	0.19	0.19	0.26
7	0.16	0.23	0.07	0.14	0.10	0.19	0.13	0.21
	0.25	0.30	-0.09	0.12	0.15	0.22	0.19	0.27
Year over Year Increase			-137.06%	-61.43%	-260.05%	86.66%	33.15%	24.71%

Bush Control Points Table								
	April 8, 2021		October 30, 2021		April 11, 2022		April 6, 2023	
Control Points	Pre NBR	Pre NDVI	Post NBR	Post NDVI	NBRp 1	NDVIp 1	NBRp 2	NDVIp 2
1	0.25	0.30	-0.02	0.09	0.09	0.11	0.12	0.13
2	0.19	0.24	-0.13	0.09	0.14	0.20	0.20	0.23
3	0.26	0.31	0.06	0.12	0.06	0.17	0.12	0.22
4	0.30	0.35	-0.07	0.10	0.18	0.24	0.21	0.28
5	0.22	0.30	-0.03	0.14	0.15	0.23	0.16	0.27
6	0.30	0.36	-0.16	0.10	0.05	0.20	0.22	0.30
7	0.34	0.36	-0.08	0.13	0.24	0.37	0.25	0.29
	0.27	0.32	-0.06	0.11	0.13	0.22	0.18	0.25
Year over Year Increase			-123.49%	-65.60%	-307.63%	98.23%	41.76%	13.03%